Mineralogy and Petrology (2005) 83: 87–112
DOI 10.1007/s00710-004-0060-6

Mineralogy and Petrology
Printed in Austria

Hydrothermal alteration of oceanic crust in the West Philippine Sea Basin (Ocean Drilling Program Leg 195, Site 1201): inferences from a mineral chemistry investigation

M. D'Antonio[1] and **M. B. Kristensen**[2]

[1] Dipartimento di Scienze della Terra, University Federico II, Napoli, Italy
[2] Department of Earth Sciences, University of Aarhus, Denmark

Received January 7, 2004; revised version accepted August 18, 2004
Published online October 20, 2004; © Springer-Verlag 2004
Editorial handling: J. P. Eissen

Summary

Secondary minerals of a 91 meters-thick sequence of pillow basalts cored during ODP Leg 195 (Site 1201, West Philippine Basin) were investigated to reconstruct the hydrothermal alteration history and regime. The basement was first buried by red clays, and then by a thick turbidite sequence, thereby isolating it from seawater. The basalts are primitive to moderately fractionated, texturally variable from hypocrystalline and spherulitic to intersertal, sub-ophitic and intergranular. Relic primary minerals are plagioclase, clinopyroxene and opaques. Hydrothermal alteration pervasively affected the basalts, generating secondary clay minerals (mostly glauconite, minor Al-saponite and Fe-beidellite), ''iddingsite'', Ca–Na-zeolites, minor alkali-feldspar and calcite. The secondary mineral paragenesis and mutual relationships suggest that the hydrothermal alteration occurred under zeolite-facies conditions, at temperatures <100–150 °C. The main phase of alteration occurred under oxidizing conditions, with a high seawater/rock ratio, in an open-circulation regime, at temperatures of 30–60 °C, with precipitation of abundant glauconite and ''iddingsite''. A later stage of alteration occurred at ca. 70 °C, with precipitation of abundant Ca–Na-zeolites and minor calcite, in a more restricted circulation regime as a consequence of basement burial under the sedimentary cover, which supplied an altered, Ca-rich and Mg–K-sulfate-poor water causing precipitation of almost pure calcite.

Introduction

Mineralogical and geochemical studies of drilled or dredged mid-ocean ridge basalts (MORB) have shown that the secondary mineral paragenesis is strongly indicative of the conditions under which the hydrothermal alteration has occurred. In particular, association of specific phases (e.g., Mg–Fe–K-bearing clay minerals, zeolites, carbonates, epidotes, amphiboles) sensitive to thermo-baric parameters can provide useful information on the temperature and oxygen fugacity conditions of the alteration environment (*Humphris* and *Thompson*, 1978a; *Honnorez*, 1981; *Alt* and *Honnorez*, 1984; *Alt* et al., 1986; *Laverne* et al., 1996; *Teagle* et al., 1996; *Alt*, 1999; *Pichler* et al., 1999; *Hunter* et al., 1999; *Marescotti* et al., 2000).

The hydrothermal regime in the oceanic environment has been shown to change significantly with the distance from the ridge axis (*Lister*, 1982). In the active convection cells located at the spreading axes, high amounts of heat are provided by a magma chamber or cooling plutonic rocks. Thus, at ridge axes the temperatures of seawater-derived fluids are high (>350 °C) and the fluid circulation is rapid, giving rise to high-T metamorphism (up to amphibolite facies), fluid discharge through black smokers and massive sulfide precipitation. A few kilometers away from the ridge axis, the hydrothermal regime changes to passive (off-axis) conditions, characterized by lower temperatures (<150 °C) and slower fluid circulation driven only by the cooling of the oceanic lithosphere (*Lister*, 1982; *Fehn* et al., 1983). Within the first tens of kilometers from the ridge axis highly oxidizing conditions prevail and a large amount of seawater is in contact with the basalt (open system). Further away, with progressive cooling and ageing of the oceanic lithosphere, the circulation becomes closed, i.e. the basaltic crust loses contact with seawater, as a consequence of its isolation caused by a sedimentary cover. Thus, the hydrothermal regime becomes reducing, and is characterized by a much lower fluid/rock ratio. Changes in the hydrothermal system conditions are efficiently recorded by the occurrence of secondary minerals (*Alt* and *Honnorez*, 1984; *Alt* et al., 1986; *Mottl* and *Wheat*, 1994; *Alt*, 1999).

Abundance and nature of the secondary minerals are shown to correlate with geochemical features of the rocks, such as loss on ignition (L.O.I.) and many major and trace element contents (*Humphris* and *Thompson*, 1978b; *Alt* et al., 1986; *Laverne* et al., 1996; *Pichler* et al., 1999; *Bach* et al., 2001), as well as radiogenic and stable isotopes (*Alt* et al., 1995; *Agrinier* et al., 1995; *Teagle* et al., 1996, 1998; *Alt* and *Teagle*, 2003). These studies are of basic importance for investigations aimed at defining the geochemical element and fluid fluxes in hydrothermal zones, as well as geochemical mass balance in specific environments, such as mid-ocean ridges, arc, and back-arc zones (*Mottl* and *Wheat*, 1994; *Shikazono* et al., 1995; *Zierenberg* et al., 1995; *Laverne* et al., 2001; *Wetzel* et al., 2001; *Alt* and *Teagle*, 2003).

During Ocean Drilling Program Leg 195, 91 meters of presumably 49 Ma old oceanic crust has been cored at Site 1201, located in the West Philippine Basin, west of a submerged paleo-arc, the Palau-Kyushu Ridge (Fig. 1; *Salisbury* et al., 2002). The cored sequence of basaltic pillow and sheet lavas along with hyaloclastite breccia, is pervasively altered, although with decreasing intensity down hole (*Salisbury* et al., 2002).

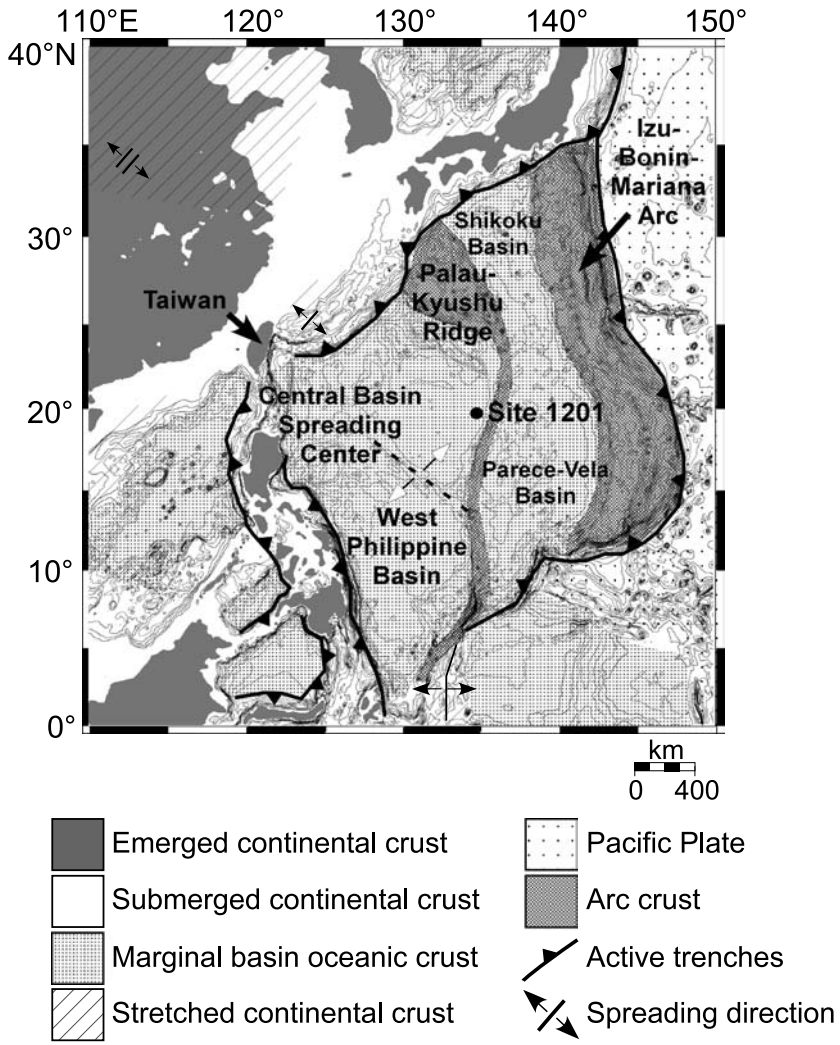

Fig. 1. Map of the West Pacific ocean (made using the GMT database) which shows the location of ODP Site 1201 in relation to the main tectonic features of the area, particularly fossil and active volcanic arcs, marginal basins and spreading centers. Areas with different types of crust are indicated with different patterns, according to *Rangin* et al. (1995)

A mineral chemistry investigation using electron microprobe analysis was performed with the aim of defining the nature and chemical variability of secondary minerals, in order to constrain the hydrothermal alteration history and conditions. This information is used to infer the water-rock ratio, the temperature at which alteration occurred, and the composition of fluids involved in the alteration after the emplacement of the West Philippine Basin basement at Site 1201.

Even though the investigated sequence is representative only of the uppermost part of the layer 2a at Site 1201, it is commonly acknowledged that this portion of the oceanic crust is the most important supplier of metasomatic fluids to subduction zones (*Mottl* and *Wheat*, 1994; *Alt*, 1999). Thus, comprehension of alteration

pattern and processes affecting the uppermost portion of the oceanic crust is fundamental in any study of the chemical recycling in subduction zones.

Geological setting

The Philippine Sea Plate, enclosed between the converging Eurasian and Pacific plates, includes three back-arc basins: the West Philippine Basin, the Shikoku Basin and the Parece-Vela Basin (Fig. 1). The West Philippine Basin is the result of slow opening along the Central Basin Spreading Center, which has been active during at least two stages of rifting, the first of which was oriented in a northeast-southwest direction since approximately 58 until 45–42 Ma ago (*Hilde* and *Lee*, 1984; *Hall* et al., 1995; *Fujioka* et al, 1999; *Deschamps* et al., 2002). In the same period, boninitic lavas were erupted to the east in response to initiation of subduction of the Pacific Plate beneath the Philippine Sea Plate (*Hall*, 2002). Since 45 Ma ago in the Middle Eocene, the Philippine Sea Plate had rotated by $\sim 50^\circ$ clockwise and drifted to the north (*Hall* et al., 1995). At about the same time (42 Ma ago, according to *Hussong* and *Uyeda*, 1981), the spreading direction shifted to north–south and opening of the West Philippine Basin continued. Meanwhile, volcanic activity was sustained along the Palau-Kyushu Ridge (Fig. 1), a volcanic arc located along the eastern margin of the West Philippine Basin, representing a precursor of the present-day Izu-Bonin-Mariana Arc, until at least 35 Ma ago (*Hall* et al., 1995; *Salisbury* et al., 2002).

Spreading along the Central Basin Spreading Center ceased about 35 Ma ago according to *Hilde* and *Lee* (1984), but more recent studies suggest that late stage spreading and/or volcanism may have continued until 26 Ma ago (*Deschamps* et al., 1999, 2002; *Fujioka* et al., 1999; *Okino* et al., 1999) in response to opening of the Parece-Vela and Shikoku basins to the east. These basins formed as a consequence of renewed subduction and hinge roll-back of the Pacific Plate along the eastern Philippine Sea Plate margin, which initiated east–west rifting (*Hall*, 2002; *Deschamps* et al., 2002) separating the Palau-Kyushu Ridge from the Izu Bonin-Mariana Arc. Since 26 Ma ago the Parece-Vela and Shikoku basins were fully developed as extensional back-arc basins and the inactive Palau-Kyushu Ridge was submerged. According to *Hall* et al. (1995), the second phase of 40° clockwise rotation began 25 Ma ago. Spreading in the Parece-Vela and Shikoku basins ceased 15 Ma ago when the Philippine Sea Plate continued its clockwise rotation and northern path to its present-day position.

Ocean Drilling Program Site 1201 is situated in the West Philippine Basin at $19^\circ 17.8'$N, $135^\circ 5.9'$E, approximately 100 km west of the now submerged volcanic arc, Palau-Kyushu Ridge (Fig. 1). According to magnetic lineation interpretation (*Hilde* and *Lee*, 1984), although not confirmed by paleontological evidence (*Salisbury* et al., 2002), the volcanic basement at Site 1201 is approximately 49 Ma old and formed during the initial stage of northeast-southwest rifting along the Central Basin Spreading Center. Approximately 91 meters have been cored into the basement starting from 509 meters below sea floor (mbsf; Fig. 2). Calm marine sedimentation covered the volcanic basement with a 2.5-m-thick claystone in the Late Eocene (>34.3 Ma; *Salisbury* et al., 2002). During the Late Eocene and until the Early Oligocene (>34.3–30 Ma), turbidity currents deposited

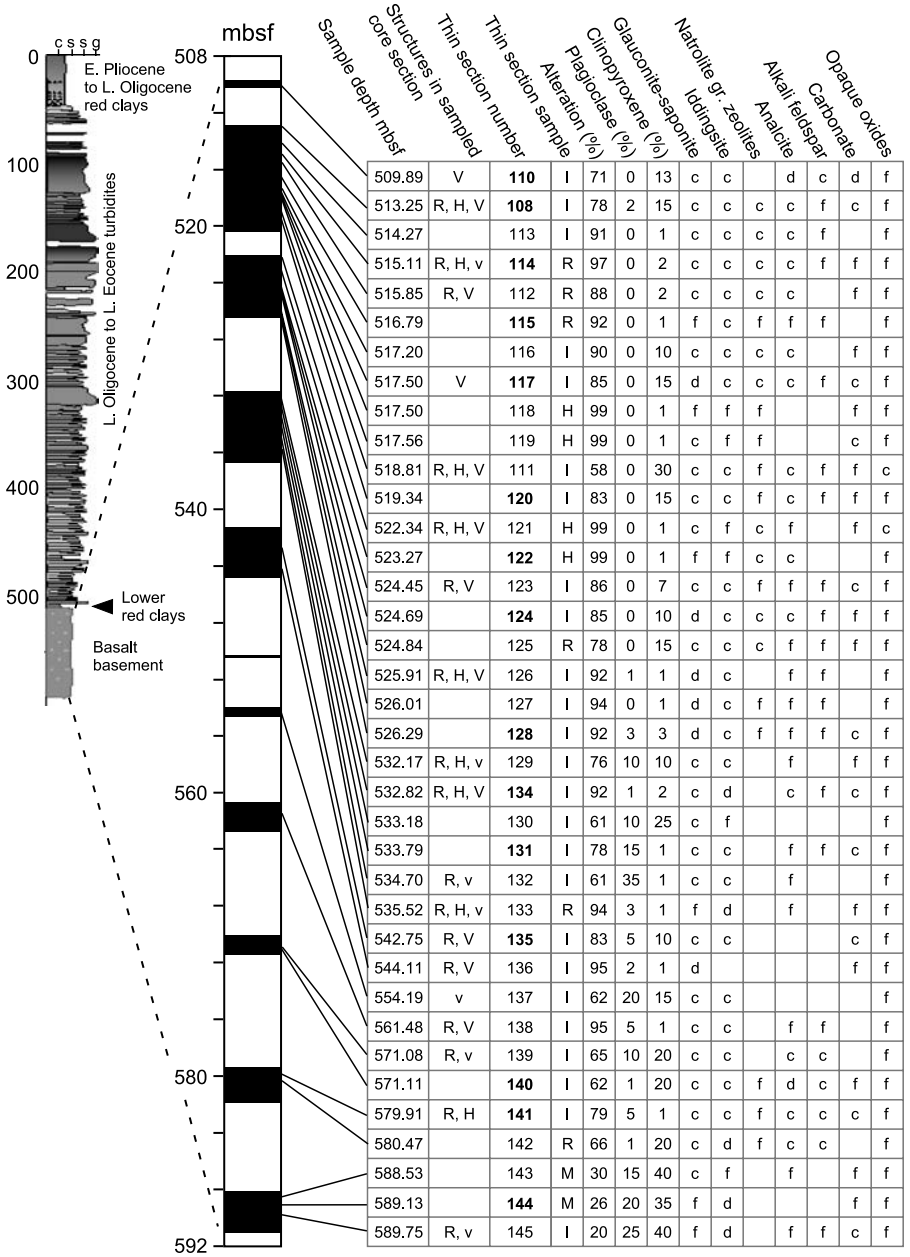

Sample depth mbsf	Structures in sampled core section	Thin section number	Thin section sample	Alteration (%)	Plagioclase (%)	Clinopyroxene (%)	Glauconite-saponite	Natrolite gr. - zeolites	Iddingsite	Alkali feldspar	Analcite	Carbonate	Opaque oxides
509.89	V	**110**	I	71	0	13	c	c		d	c	d	f
513.25	R, H, V	**108**	I	78	2	15	c	c	c	c	f	c	f
514.27		113	I	91	0	1	c	c	c	c	f		f
515.11	R, H, v	**114**	R	97	0	2	c	c	c	c	f	f	f
515.85	R, V	112	R	88	0	2	c	c	c	c		f	f
516.79		**115**	R	92	0	1	f	c	f	f	f		f
517.20		116	I	90	0	10	c	c	c	c		f	f
517.50	V	**117**	I	85	0	15	d	c	c	c	f	c	f
517.50		118	H	99	0	1	f	f	f			f	f
517.56		119	H	99	0	1	c	f	f			c	f
518.81	R, H, V	111	I	58	0	30	c	c	f	c	f	f	c
519.34		**120**	I	83	0	15	c	c	f	c	f	f	f
522.34	R, H, V	121	H	99	0	1	c	f	c	f		f	c
523.27		**122**	H	99	0	1	f	f	c	c			f
524.45	R, V	123	I	86	0	7	c	c	f	f	f	c	f
524.69		**124**	I	85	0	10	d	c	c	c	f	f	f
524.84		125	R	78	0	15	c	c	c	f	f	f	f
525.91	R, H, V	126	I	92	1	1	d	c		f	f		f
526.01		127	I	94	0	1	d	c	f	f	f		f
526.29		**128**	I	92	3	3	d	c	f	f	f	c	f
532.17	R, H, v	129	I	76	10	10	c	c		f		f	f
532.82	R, H, V	**134**	I	92	1	2	c	d		c	f	c	f
533.18		130	I	61	10	25	c	f					f
533.79		**131**	I	78	15	1	c	c		f	f	c	f
534.70	R, v	132	I	61	35	1	c	c		f			f
535.52	R, H, v	133	R	94	3	1	f	d		f		f	f
542.75	R, V	**135**	I	83	5	10	c	c				c	f
544.11	R, V	136	I	95	2	1	d					f	f
554.19	v	137	I	62	20	15	c	c					f
561.48	R, V	138	I	95	5	1	c	c		f	f		f
571.08	R, v	139	I	65	10	20	c	c		c	c		f
571.11		**140**	I	62	1	20	c	c	f	d	c	f	f
579.91	R, H	**141**	I	79	5	1	c	c	f	c	c	c	f
580.47		142	R	66	1	20	c	d	f	c	c		f
588.53		143	M	30	15	40	c	f		f		f	f
589.13		**144**	M	26	20	35	f	d				f	f
589.75	R, v	145	I	20	25	40	f	d		f	f	c	f

Fig. 2. Core summary showing the distribution of primary and secondary minerals with depth in basement rocks from Site 1201. The scheme of the sedimentary sequence cored at Hole 1201D, with grain size scale (clay, silt, sand, and gravel) at top, shows the two major lithological units, i.e. red clays and turbidites, above the volcanic basement. Dashed lines show an enlargement of the cored basement sequence. Black boxes represent recovered cores. Lines from the core section point to sample depth in the core (mbsf). "Structure in sampled core section" is based on visual core descriptions and denotes intervals where pillow rims (R), hyaloclastite (H), or veins (V = common, v = few) are observed. Thin section numbers in bold are those used for microprobe analysis in this study. Thin section samples have been divided into pillow rims (R), pillow interiors (I), hyaloclastite (H), and massive basalt (M). Alteration and mineralogy are based on visual thin section observations. Total alteration and preserved primary phases are given in percent by volume. Secondary mineral phases are classified as few (f = 1–3%), common (c = 3–5%), or dominant (d = 5–10%)

~450 meters of sandstone, silty claystone, breccia and claystone (53–509 mbsf). These turbidites consist of detrital volcaniclastic material from the Palau-Kyushu Ridge and clasts derived from surrounding carbonate reefs. The turbidite sequence evolved from low-energy turbidite currents in the lower part to high-energy turbidite currents in the upper part. Subsidence of the Palau-Kyushu Ridge brought the turbidite sedimentation to an end, after which pelagic sedimentation resumed with deposition of ~53 meters of clays, cherts, and interbedded sandstones and silty claystones, between the Late Oligocene and Early Pliocene (*Salisbury* et al., 2002).

Samples and analytical techniques

Sample description

Mainly pillow lava basalts, perhaps one sheet lava flow unit, as well as several hyaloclastite fragments were cored during ODP Leg 195 at Site 1201. Of the 91.4 meters drilled into the basement, ~32% was recovered on the whole. The upper part of the basement, from 508.9 until 544 mbsf, had exceptionally good drill recovery (>55%), while less was recovered from the lower part (Fig. 2). Chilled glassy pillow margin rims, hyaloclastite and inter-pillow sedimentary material were observed throughout the recovered sequence. During Leg 195 the basement sequence was extensively sampled for petrographic and geochemical studies. Pillow interiors, pillow margins and hyaloclastite fragments were selected for shipboard preparation of the thin sections used in this study.

The basalt is generally fine-grained with none or very few phenocrysts mainly of altered plagioclase, although rare olivine pseudomorphs also occur. Alteration is greatest in the upper cores closest to the pelagic clay contact and decreases significantly only in the lowermost cores (Fig. 2).

The devitrified glassy groundmass gives the upper cores a ''rosette'' texture, whereas in the lower cores the groundmass appears more micro-crystalline. The lowermost part of the recovered sequence, from about 588 to 590 mbsf, is more massive and presumably consists of a sheet lava flow unit. The grain size is slightly coarser, the alteration is markedly less (below 30%), and no pillow rims were observed. Pillow rims are, however, observed in the same core immediately under the sheet lava flow unit.

The abundance of vesicles in the basalts varies throughout the sequence but is greatest in the upper part and close to chilled pillow margins, where vesicles are seen to coalesce and form outward radiating patterns. Some vesicles have been completely or partially occupied by secondary mineral phases such as clay minerals, zeolites and less frequently, carbonate. Veins are also more abundant in the upper cores and often contain inter-pillow sedimentary material and palagonitized, angular glass shards. In the lower cores, veins are commonly thinner and have clay mineral linings and zeolite or carbonate fillings. Commonly veins are composite, having a later stage of carbonate precipitation overprinting earlier clay mineral deposition. Thermal contraction fracture patterns also containing a carbonate precipitate were observed in two cores, 195-1201D-49R-1 (541.3 mbsf) and 195-1201D-53R-1 (570.3 mbsf).

Hyaloclastite samples are composed of inter-pillow sedimentary material (red clays containing marine bioclasts) and completely altered angular glass shards. Colloidal clays and zeolites replace the original glass constituting the shards.

Based on major and trace element geochemistry (*Salisbury* et al., 2002), the basement rocks of Site 1201 are classified as tholeiitic basalt. They are characterized by relatively high MgO (8.9–5.8 wt.%), Cr (460–324 ppm) and Ni (168–71 ppm) contents, and Mg# (molar Mg/[Mg + Fe]∗100, 68–55), thus varying from primitive to moderately fractionated. However, since most samples are highly altered, as testified also by their high L.O.I. contents (0.9–6.6 wt.%; *Salisbury* et al., 2002), and due to the mobility of Mg in altered basaltic rocks, the MgO content and Mg# parameter are not suitable indicators for the degree of chemical evolution of the magma. On the basis of Ti, Zr and Y relationships, the basalts display geochemical features intermediate between those typical of mid-ocean ridge basalts and island arc tholeiites (*Salisbury* et al., 2002), in agreement with similar basalts dredged from the Central Basin Spreading Center (*Fujioka* et al., 1999), thus confirming their back-arc origin.

Investigation methods and analytical techniques

A total of 37 thin sections representative of the recovered cores of basement at Site 1201, Hole D (26 pillow interior/sheet lava, 7 pillow margin, and 4 hyaloclastite samples) were studied using a petrographic microscope. The primary and secondary mineral content, the various textures, veins and vesicles were examined in order to characterize the petrography of all samples and constrain the down-hole hydrothermal alteration pattern. The total degree of alteration varies from 20 to 96% in the investigated samples assumed to be pillow interiors, with least alteration found in samples below 580 mbsf. Alteration in pillow rim samples varies between 66 and 97% and likewise, the lowest core samples are the least altered (Fig. 2).

The secondary minerals of pillow basalts, massive basalts, and hyaloclastite from Site 1201 were analyzed by electron microprobe in 14 carbon-coated polished thin sections provided by the Ocean Drilling Program (West Coast Repository, Scripps Institution of Oceanography, La Jolla, CA, U.S.A.). The investigated samples are representative of the main basement units recognized during shipboard investigations (*Salisbury* et al., 2002), and are distributed throughout the recovered cores. Electron microprobe analyses (EMPA) were performed using the Cameca Camebax Microbeam of the C.N.R. – Centro di Studi per la Geodinamica Alpina (Padova, Italy), equipped with four vertical WDS X-ray spectrometers and one EDS spectrometer. The analytical conditions of the electron beam voltage and current were set to 15 kV and 10 nA, respectively; the beam was enlarged to a diameter of 5 μm, and the counting times set to 10 sec for both peak and background. Alkalis were measured first in the routine to prevent their loss under the electron beam; further prevention for loss of alkalis in zeolites was achieved by moving the stage slightly around during acquisition. Data were reduced using a ZAF correction procedure. Both natural and synthetic standards were employed to check the precision and accuracy performances of the machine.

Raman microspectroscopy techniques were used in order to establish which calcium carbonate polymorphs were present in the investigated rocks. Carbonates found in six thin sections from different cores drilled into the basement sequence were analyzed with a Labram Jobin-Yvon LTD Raman spectrometer equipped with a laser Ar^+ ($\lambda = 514.5$ nm), at the Dipartimento di Scienze della Terra, University of Siena, Italy. Analytical conditions were: emission power, 300 mW; accumulation times, 10 sec.

Petrography

Textural features and primary mineralogy

Variable textures were observed in pillow rim and pillow interior samples. In pillow margin fragments, e.g. Sections 195-1201D-46R-2, 46R-3 and 48R-4, distinct concentric zones were recognized and interpreted as the result of fast cooling conditions. These zones are: i) an outermost glassy zone, the so-called chilled margin, characterized by sparse, dark brown spherulites enclosed within large patches of light yellow palagonitized glass; ii) an intermediate dark brown zone, with closely packed spherulites; iii) an innermost reddish zone, where brown-reddish spherulites and the first plagioclase microliths occur; iv) a more crystalline interior, with mainly spherulitic, intersertal and subophitic textures. The first three zones account for the first 1–2 centimeters of the pillow margin, and the transition among them is gradual. No actual holocrystalline pillow core has been found; however, textures within the pillow interiors in addition to spherulitic (the ''rosette'' texture visible in hand-specimen), intersertal, and subophitic textures, also include hyalopilitic, branching, felty and intergranular textures. Some of these textures can be attributed to fast cooling of lava (*McPhie* et al., 1993); additional features confirming this interpretation are ''swallow-tailed'' plagioclase, ''feather-like'' clinopyroxene, and undulatory extinction of subhedral clinopyroxene.

The primary paragenesis observed in the basalts includes plagioclase, olivine, clinopyroxene and opaque minerals. Clinopyroxene is the only well-preserved phase throughout the core, with few cases of recrystallization. Clinopyroxene is a Mg-rich augite, generally containing high amounts of Cr_2O_3.

Combinations of clay minerals, iron oxyhydroxides and sometimes carbonates replace olivine phenocrysts and microphenocrysts throughout the cores. Plagioclase is mostly completely altered above 534 mbsf, commonly replaced by zeolites and alkali-feldspar, and less commonly by clay minerals and/or carbonates. Na-rich rims are frequently preserved; these, in conjunction with the Ca-rich cores preserved in the least altered samples, point to an original chemical zoning from bytownite to andesine. Primary, euhedral opaque minerals are Ti-magnetite and more rarely Cr-spinel (*D'Antonio* and *Kristensen*, 2004). The abundance of phenocrysts is generally less than 2% by volume and never exceeds 7% by volume (*Salisbury* et al., 2002).

The textural relationships among the primary phases indicate that plagioclase and olivine were the first phases to crystallize, followed by clinopyroxene and finally opaque minerals (*Salisbury* et al., 2002; *D'Antonio* and *Kristensen*, 2004), as typically found in MOR tholeiites.

Petrography of secondary minerals

All the investigated rock samples display some degree of alteration, though variable, being lowest in massive basalt cores, and highest in glassy pillow rims. According to the textural occurrence of secondary minerals, four types of alteration can be distinguished: i) pseudomorphic replacement of primary minerals; ii) transformation of glassy groundmass into combinations of zeolites and clay minerals (''palagonitization''); iii) filling of primary vesicles; iv) occurrence of crosscutting veins and hyaloclastite breccia cements. On the basis of optical characteristics, four main groups of secondary minerals were recognized (*Salisbury* et al., 2002; present work): clay minerals (smectites and smectite/iron oxyhydroxide mixtures); zeolites (including analcite); alkali-feldspars and carbonates. In addition, secondary opaque minerals occur throughout the basement sequence.

Clay minerals are the most dominant secondary mineral group throughout the core (Fig. 2). They occur mainly as patches in the glassy groundmass, and as pseudomorphic replacement of plagioclase and olivine crystals (Fig. 3E), alone or accompanied by other secondary minerals, such as zeolites and/or carbonates. Clay minerals also occur as lining and/or filling of vesicles (Fig. 3A) and as thin veins in the pillow and sheet lavas (Fig. 3F). Observed in plane-polarized light (PPL), they appear with pale to bright colors, variable from green, to yellow and brown, to red, giving green or red-brown tints to the rocks in hand-specimen. ''Zoned'' vesicles, filled with clay minerals changing in color from either green to yellow-brown, or red to brown from rim to core, were frequently observed. According to on-board XRD analyses made on a few basalt samples, two types of clay minerals are present in the basement rocks, characterized by 12 and 15 Å peaks, respectively (*Salisbury* et al., 2002). EMPA revealed that these clay minerals belong to the K– and Mg–Fe-rich smectites, and mixtures of smectites with variable amounts of iron oxyhydroxides (named ''iddingsite'' after the literature; Fig. 3C, E).

Zeolites are also common secondary phases, occurring both as replacement of plagioclase, alone or in conjunction with secondary alkali-feldspar, and filling vesicles and veins. They occur either as platy or as fibrous and acicular crystals. Optically, two zeolite groups were distinguished (Fig. 3A–D) and EMPA revealed that these are natrolite-group zeolites and analcite, respectively, as also confirmed by shipboard XRD analyses made during Leg 195 (*Salisbury* et al., 2002).

Secondary alkali-feldspar is a common alteration product after plagioclase phenocrysts and microphenocrysts, often in conjunction with analcite (Fig. 3D). It has been identified optically as sanidine (*Salisbury* et al., 2002), although its composition is variable, approaching that of albite (see next section).

Carbonates are common secondary minerals, although less abundant than clay minerals and zeolites. They occur as replacement of plagioclase and olivine, always accompanying zeolites, and as vein filling or patches within the groundmass (Fig. 3D–F).

Other secondary minerals are: 1) opaque minerals, occurring as skeletal or sometimes euhedral microphenocrysts after olivine, or as fine ''dust'' dispersed within the altered groundmass; in the latter case, they are commonly observed lining clay mineral spherulites indicating that Fe and Ti have been expelled from

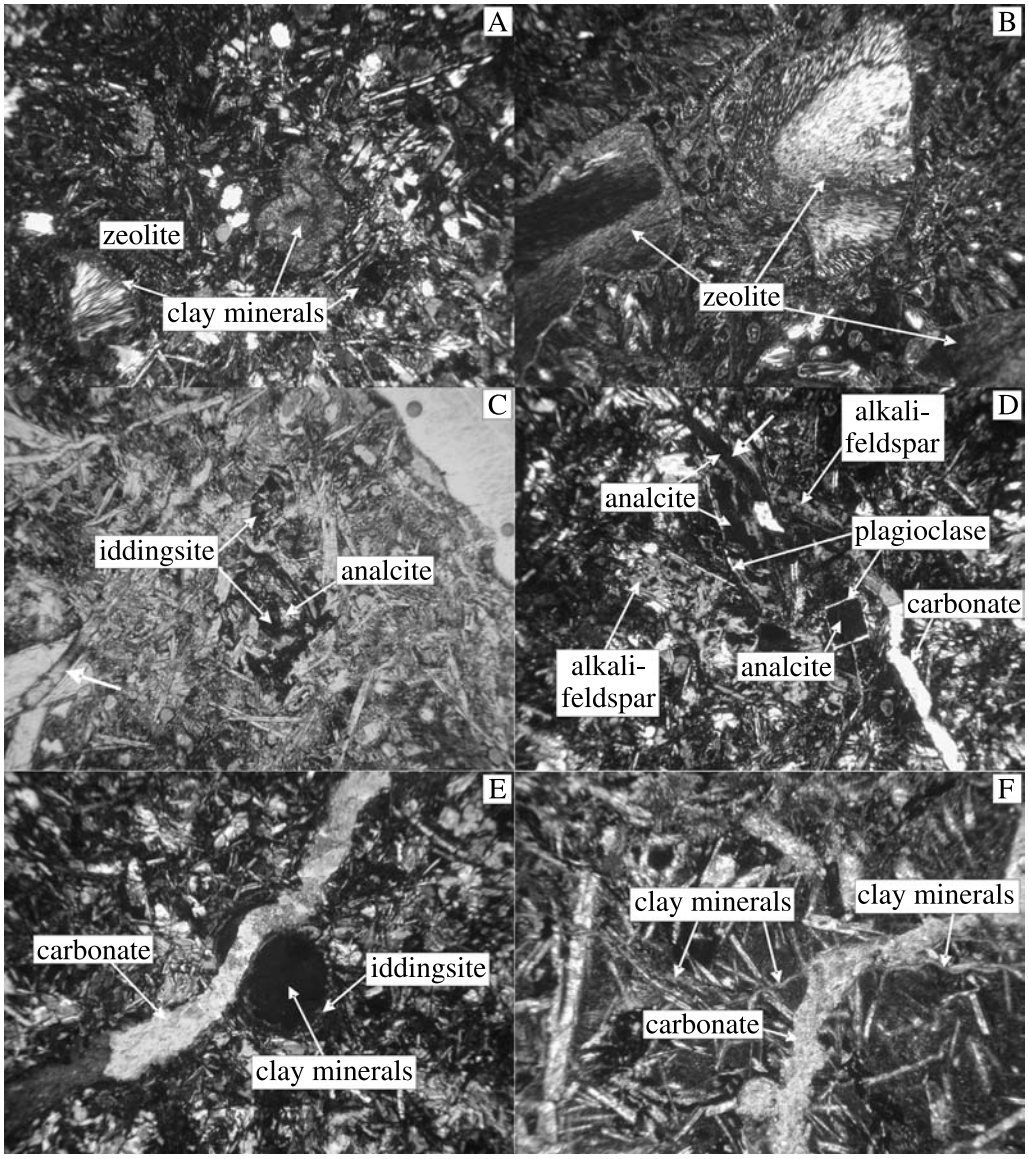

Fig. 3. Photomicrographs showing the main alteration minerals occurring in Site 1201 basalts. **A** clay minerals in amygdules and patches in groundmass; notice amygdule to the left, with clay mineral lining and Na–Ca-zeolite filling; core 195-1201D-46R-4, 24–27 cm, cross-polarized light (XPL), magnification 5×; **B** Na–Ca-zeolite filling amygdules without clay mineral lining; core 195-1201D-46R-4, 24–27 cm, XPL, magnification 5×; **C** ''iddingsite'' and analcite after former olivine crystals; notice the late-stage vein crosscutting an altered plagioclase to the lower left (thick white arrow); core 195-1201D-45R-5, 103–107 cm, plane-polarized light (PPL), magnification 5×; **D** alkali-feldspar and analcite after plagioclase crystals; the thin, light-colored rim is of fresh plagioclase; the composite analcite/carbonate veinlet, crosscutting an altered plagioclase, is the same as in Fig. 3C; core 195-1201D-45R-5, 103–107 cm, XPL, magnification 5×; **E** late-stage carbonate vein crosscutting an olivine pseudomorph; core 195-1201D-55R-2, 19–20 cm, XPL, magnification 5×; **F** late-stage carbonate vein crosscutting a thin clay-mineral vein; core 195-1201D-48R-2, 38–41 cm, PPL, magnification 5×

the original glassy matrix during the palagonitization process; moreover, primary magnetite crystals are partly maghemitized and 2) rare recrystallized clinopyroxene, recognizable by its anomalously high TiO_2 and Na_2O contents, up to 1.8 and 0.6 wt.%, respectively (*D'Antonio* and *Kristensen*, 2004; *Laverne* et al., 1995).

Distribution of secondary minerals with depth

Figure 2 illustrates the down-hole distribution of the main secondary minerals occurring in the investigated samples. A general decrease in alteration intensity can be observed down-hole at Site 1201, particularly in the lowermost cores. This implies that the major control on alteration was proximity to the basement-seawater interface, and that the influence of seawater (i.e., cumulative seawater/rock ratio) decreased with depth. However, it must be pointed out that the abundance of secondary minerals with depth appears to be controlled also by the texture and lithology, namely whether the host rock is a pillow rim, pillow interior, or more massive lava. Thus, within the glassy pillow rims and hyaloclastite fragments, the degree of alteration is higher; within more massive lava, it is lower. Moreover, at the scale of hand specimen, the distribution of secondary minerals is strongly controlled by the presence of fractures that are preferential pathways allowing more rapid penetration of fluids into the rocks. For instance, oxidation halos in the basalt occur adjacent to veins filled with interpillow sedimentary material. These halos consist of vesicle-rich altered basalt; at the contact with the vein vesicles are mostly filled with reddish-brown clay minerals (including mixtures with Fe oxyhydroxides), whereas vesicles within a few centimeters from the vein are filled with green-yellow clay minerals. Otherwise, clay minerals along with secondary opaque minerals occur as replacement of primary glass, throughout the basement sequence. However, clay minerals replacing glass appear to be incompletely crystallized.

Zeolites are generally much less abundant below 534 mbsf, in relation to a reduced amount of vesicles and the common occurrence of preserved plagioclase in the rocks; above this depth, fresh plagioclase occurs sporadically. Carbonate and alkali-feldspar do not have a particular distribution pattern, being just sparsely present throughout the sequence.

Results of electron microprobe measurements

Representative EMP analyses of secondary minerals and glass of ODP Leg 195 Site 1201 basalts are listed in Tables 1 through 3; all the analyses performed are plotted in the diagrams of Figs. 4 through 8. The entire analytical set can be provided upon request.

Clay minerals and iron oxyhydroxides

A selection of EMP analyses of all texturally and chemically different clay minerals found in Site 1201 rocks is reported in Table 1. On the basis of the main textural and chemical features, three types of clay minerals were distinguished, named Type 1, Type 2 and Type 3, the first being tri-octahedral, the second and

Table 1. *Representative microprobe analyses of different types of clay minerals and "iddingsite". Formulae of clay minerals Type 1 (Al-saponite) calculated assuming all Fe as Fe^{2+}; formulae of clay minerals Type 2 (glauconite), Type 3 (Fe-beidellite), "iddingsite" (Idd) and mixtures among the three end-members (Mix) calculated assuming all Fe as Fe^{3+}.* b.d.l. *below detection limit*

Label	128-124-4	140-56-1	135-110-5	115-128-2	134-101-3	134-103-4	144-123-10	134-103-3	134-101-4	134-101-5	144-122-3	131-55-2
Occurrence	yellow clay after ol	green clay patch in the groundmass	green clay patch in the groundmass	red clay "rosette" in the groundmass	red clay patch in the groundmass	green clay patch in the groundmass	red clay patch in the groundmass	brown clay patch in the groundmass	red clay after ol	red clay after ol	red clay after ol	red clay after ol
Type	Type 1	Type 2	Type 2	Type 3	Mix	Mix	Mix	Mix	Mix	Mix	Idd	Idd
SiO_2	45.35	46.99	48.69	46.21	47.66	46.07	24.86	21.33	40.03	33.30	6.99	10.13
TiO_2	b.d.l.	b.d.l.	b.d.l.	0.22	0.07	0.09	0.46	0.80	0.18	0.24	0.03	0.29
Al_2O_3	8.29	6.83	3.61	13.78	10.03	11.71	4.79	7.59	7.82	7.56	1.95	3.38
Cr_2O_3	0.09	b.d.l.	0.05	0.03	b.d.l.	b.d.l.	b.d.l.	b.d.l.	b.d.l.	0.04	0.04	0.10
FeO	11.73	23.63	21.27	13.43	7.45	17.28	42.46	45.14	31.99	39.30	68.55	59.57
MnO	0.29	0.09	0.06	0.08	0.24	0.43	0.35	0.83	0.13	0.30	0.38	0.30
MgO	18.65	3.96	7.14	5.19	15.98	11.48	10.56	6.65	3.49	3.60	1.30	2.70
CaO	2.07	1.21	0.59	2.21	2.95	2.61	2.40	2.12	1.54	1.63	1.07	2.02
Na_2O	0.19	0.17	0.12	0.13	0.49	0.19	0.18	0.12	0.21	0.16	0.56	0.04
K_2O	0.03	6.74	7.74	5.26	0.34	2.40	0.08	0.66	5.25	4.06	0.03	0.15
Sum	86.70	89.65	89.29	86.54	85.20	92.28	86.12	85.26	90.65	90.19	80.91	78.68
Si	3.422	3.577	3.713	3.483	3.509	3.280	2.177	1.929	3.128	2.716	0.589	1.108
$Al^{(IV)}$	0.578	0.423	0.287	0.517	0.491	0.720	0.494	0.809	0.720	0.727	0.171	0.435
Fe^{3+}	0.000	0.000	0.000	0.000	0.000	0.000	1.329	1.263	0.153	0.557	3.240	2.457
Sum of (IV)	4.000	4.000	4.000	4.000	4.000	4.000	4.000	4.000	4.000	4.000	4.000	4.000
$Al^{(VI)}$	0.159	0.190	0.037	0.706	0.379	0.263	0.000	0.000	0.000	0.000	0.000	0.000
Fe^{2+}	0.740	0.000	0.000	0.000	0.000	0.000	0.000	0.000	0.000	0.000	0.000	0.000
Fe^{3+}	0.000	1.354	1.221	0.762	0.413	0.926	1.468	1.808	1.728	1.855	2.699	2.444
Mn	0.018	0.006	0.004	0.005	0.015	0.026	0.026	0.064	0.009	0.021	0.034	0.028
Ti	0.000	0.000	0.000	0.013	0.004	0.005	0.030	0.055	0.011	0.015	0.145	0.024
Mg	2.098	0.450	0.812	0.583	1.753	1.219	1.378	0.897	0.407	0.438	0.194	0.441
Cr	0.006	0.000	0.003	0.002	0.000	0.000	0.000	0.000	0.000	0.003	0.004	0.009
Sum of (VI)	3.021	1.999	2.077	2.071	2.563	2.438	2.903	2.823	2.154	2.332	3.074	2.945
Ca	0.167	0.099	0.048	0.179	0.232	0.199	0.226	0.205	0.129	0.142	0.131	0.237
Na	0.028	0.026	0.018	0.018	0.069	0.027	0.030	0.021	0.032	0.025	0.000	0.009
K	0.003	0.654	0.753	0.506	0.032	0.218	0.009	0.077	0.524	0.422	0.008	0.020
Sum interlayer	0.198	0.778	0.819	0.703	0.333	0.444	0.265	0.303	0.685	0.589	0.139	0.265
Total cations	7.220	6.777	6.896	6.773	6.897	6.883	7.167	7.126	6.839	6.921	7.214	7.211
$Fe^{2+}/(Fe^{2+}+Mg)$	0.261											
$Fe^{3+}/(Fe^{3+}+Mg)$		0.751	0.601	0.566	0.191	0.432	0.670	0.774	0.822	0.846	0.968	0.917

third di-octahedral. Structural formulae were calculated following *Teagle* et al. (1996), on the basis of $O_{10}(OH)_2$, and assuming all iron as Fe^{2+} in Type 1 clay minerals and as Fe^{3+} in Type 2 and Type 3 clay minerals. The clay mineral types can be recognized on the basis of their different total Al, interlayer K, and total octahedral cation contents as a function of the Fe/(Fe + Mg) ratio, as shown in the diagrams of Fig. 4. Their classification has been achieved by combining some discrimination diagrams presented in Fig. 5. In these diagrams, another mineral phase characterized by extremely high Fe content was distinguished, and is characterized by a brilliant to very dark red color in PPL. Chemically this phase can be

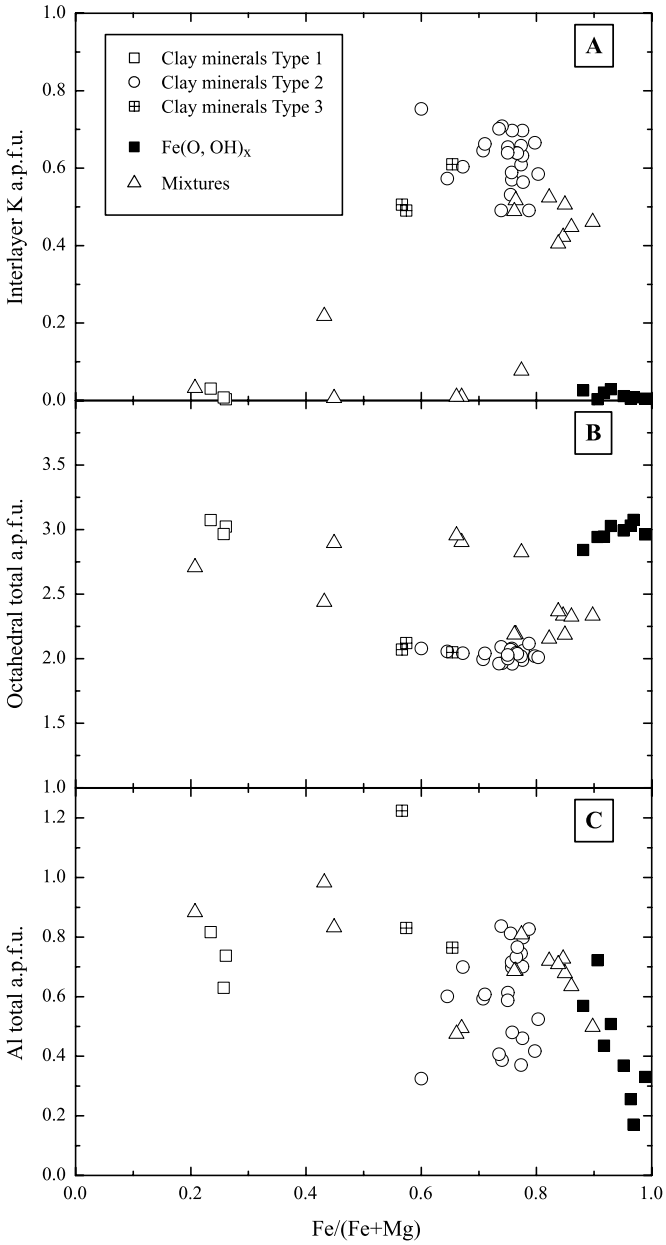

Fig. 4. Chemical features of clay minerals and clay minerals-Fe(O, OH)$_x$ mixtures of basalts from Site 1201 (data from Table 1). **A** interlayer K content vs. Fe/(Fe + Mg) ratio; **B** octahedral total content vs. Fe/(Fe + Mg) ratio; **C** Al total content vs. Fe/(Fe + Mg) ratio. *A.p.f.u.* atoms per formula unit

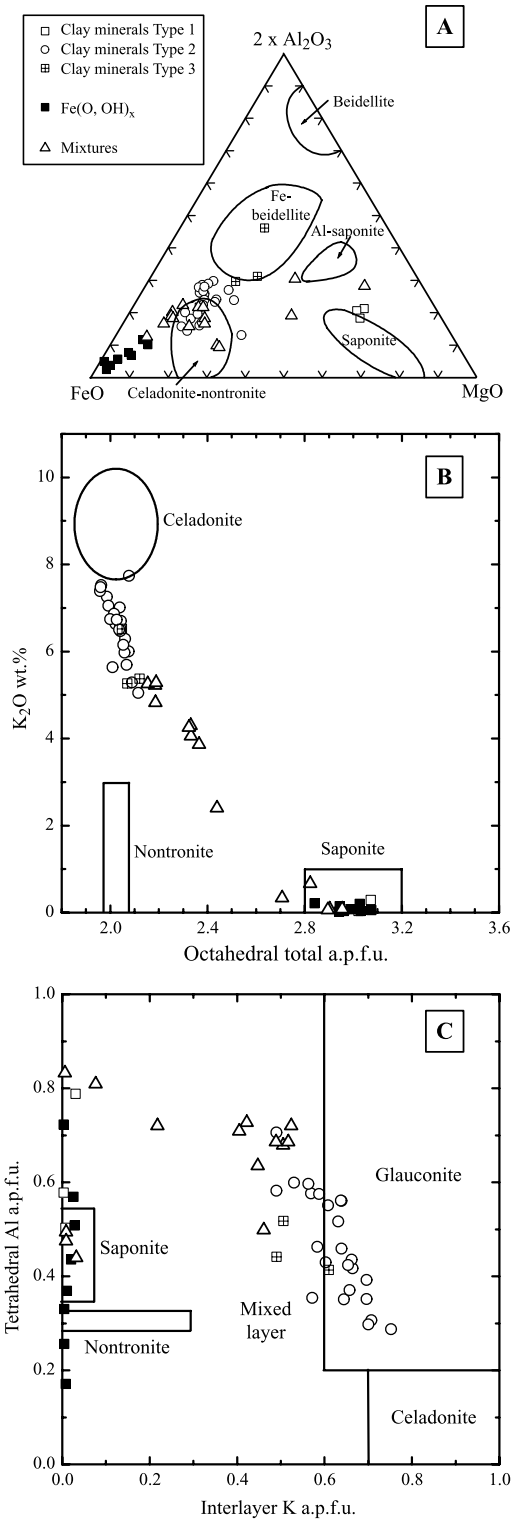

Fig. 5. Discrimination diagrams for clay minerals (data from Table 1). **A** Ternary plot FeO_{tot}–$2xAl_2O_3$–MgO (molar) (*Alt* and *Honnorez*, 1984); **B** K_2O content vs. octahedral total content; **C** tetrahedral Al content vs. interlayer K content (*Alt*, 1999). *A.p.f.u.* atoms per formula unit

ascribed to iron oxyhydroxides; in many cases it occurs as a mixture with clay minerals.

Characteristics for Type 1 clay minerals are high MgO relative to FeO_{tot} contents ($Fe/[Fe + Mg]$ in the range 0.21–0.26), high Al_2O_3 contents, and low K_2O (less than 0.4 wt.%) (Table 1 and Fig. 4). These chemical features are typical of (relatively Al-rich) saponite (Fig. 5; *Andrews*, 1980; *Alt* and *Honnorez*, 1984; *Alt*, 1999). Only three analyses belong to this type, indicating a poor saponite occurrence in the investigated rocks.

Type 2 is the most common clay mineral variety present in basalts from Site 1201. Clay minerals belonging to this type are typically bright green in color (PPL), and characterized by high $Fe/(Fe + Mg)$ ratios, in the range 0.60–0.80, high K_2O and intermediate Al_2O_3 contents (Table 1 and Figs. 4–5). Chemically these di-octahedral clay minerals can be ascribed to the celadonite group, although no pure celadonite has been detected, which is usual for weathered MORB (*Alt*, 1999 and quoted references). Instead, most Type 2 clay minerals fall within the field for glauconite in the plot interlayer K against tetrahedral Al (Fig. 5C; *Buckley* et al., 1978), or outside the field toward higher Al and lower K contents. Clay minerals Type 2, hereafter named glauconite, occur mostly filling amygdules and as patches within the groundmass (Fig. 3A), and only rarely replacing olivine. Type 3, either green- or red-colored in PPL, was found only in three occurrences, either as patches in the altered groundmass or as lining of a zeolite amygdule. It is another di-octahedral clay mineral, characterized by high Al_2O_3, intermediate K_2O contents and low $Fe/(Fe + Mg)$ ratios, and was classified as Fe-beidellite (Table 1 and Fig. 5A).

The iron oxyhydroxides occur mainly as pseudomorphic replacement of olivine (Fig. 3C, E), and have very high FeO_{tot} content, with $Fe/(Fe + Mg)$ ranging from 0.88 to 0.99, intermediate to low Al_2O_3, and low K_2O and SiO_2 contents (Table 1; Figs. 4–5). In the literature (*Alt* et al., 1993; *Laverne* et al., 1996; *Hunter* et al., 1999; *Marescotti* et al., 2000), these chemical features are referred to as ''iddingsite'', consisting of mixtures of clay minerals and iron oxyhydroxide (mixtures of goethite and hematite, $Fe(O, OH)_x$). Given the very high FeO_{tot} (56–73 wt.%) and low K_2O and SiO_2 (<0.7 and <17 wt.%, respectively; Table 1) contents, these minerals have a composition very close to that of $Fe(O, OH)_x$.

Many other analyzed clay minerals have chemical characteristics intermediate among those of Types 1, 2, 3 and iron oxyhydroxides, as is clearly seen in the plots of Figs. 4A and B. In most cases, these are mixtures of glauconite, Al-saponite and iron oxyhydroxides, showing octahedral content intermediate between 2 and 3 (Fig. 4B); tri-octahedral mixtures of Al-saponite and iron oxyhydroxides occur as well. For all these mixtures it is impossible to say whether they are chemical or mechanical mixtures of the distinct components by using EMPA alone. The positive correlation between the total amount of cations in octahedral coordination and total Fe, visible in Fig. 4B for the Fe-richest clay minerals, does however suggest the occurrence of mechanical interlayering of Fe oxyhydroxide/smectite in the clay mineral structure (*Teagle* et al., 1996; *Marescotti* et al., 2000). Only very high quality X-ray diffraction determinations or, even better, transmission electron microscopy observations, could help to unravel this problem (*Peacor*, 1992; *Li* et al., 1997).

Table 2. *Representative microprobe analyses of zeolites. Formulae calculated on the basis of 20 (natrolite-group) and 48 (analcite) oxygens, assuming all Fe as* Fe^{3+}. b.d.l. *below detection limit*

Label	114-12-3	114-13-3	117-17-1	117-23-1	117-23-3	108-116-2	110-3-1	110-2-4
Occurrence	after plagioclase	in amygdule	in glass shard	in amygdule	in amygdule	in groundmass	after plagioclase	in vein
Type	Natrolite-group	Natrolite-group	Natrolite-group	Natrolite-group	Natrolite-group	Natrolite-group	Analcite	Analcite
SiO_2	45.22	42.70	39.31	46.87	46.14	44.99	58.11	56.67
Al_2O_3	29.48	29.32	29.24	29.79	30.02	27.06	22.24	22.33
FeO	0.03	0.21	0.09	0.04	0.04	0.61	0.03	0.00
MnO	0.03	b.d.l.	0.02	0.04	0.02	b.d.l.	b.d.l.	0.52
MgO	b.d.l.	0.02	b.d.l.	b.d.l.	b.d.l.	1.48	b.d.l.	b.d.l.
CaO	4.76	11.97	12.53	8.06	5.76	11.14	0.03	0.11
Na_2O	11.16	5.62	4.11	7.56	12.44	2.10	11.92	12.15
K_2O	0.02	0.02	0.01	0.00	0.03	0.01	0.47	0.04
Sum	90.70	89.89	85.31	92.36	94.45	87.46	92.80	91.84
Si	5.703	5.480	5.316	5.770	5.637	5.813	16.652	16.461
Al	4.382	4.436	4.661	4.322	4.323	4.120	7.511	7.645
Fe^{3+}	0.003	0.022	0.010	0.004	0.004	0.066	0.006	0.000
Mn	0.003	0.000	0.002	0.004	0.002	0.000	0.000	0.129
Mg	0.000	0.005	0.000	0.000	0.000	0.285	0.000	0.006
Ca	0.644	1.647	1.816	1.063	0.754	1.541	0.010	0.035
Na	2.729	1.400	1.077	1.805	2.948	0.527	6.623	6.844
K	0.004	0.003	0.001	0.000	0.004	0.002	0.172	0.016
Total cations	13.468	12.992	12.883	12.968	13.672	12.355	30.975	31.136
Si + Al	10.085	9.916	9.977	10.092	9.960	9.934	24.163	24.106
E%	9.037	−5.258	−0.842	10.056	−3.018	0.096	10.292	10.118

Zeolites

Zeolites are the second most abundant group of secondary minerals present in Site 1201 basaltic lava and hyaloclastite. Representative EMPA data for zeolites in different occurrences are listed in Table 2. The formulae have been calculated on the basis of 20 oxygens (48 for analcite), and only those with low chemical balance, indicated by the parameter E% being less than 10 (*Passaglia*, 1970) were accepted. All the available analyses are plotted in the diagrams on Fig. 6.

The two types of zeolites distinguished on the basis of their optical properties are natrolite group zeolites and analcite. No other types of zeolites, such as phillipsite, heulandite and chabazite, also common in altered oceanic basalts elsewhere (*Alt* and *Honnorez*, 1984; *Alt* et al., 1986; *Teagle* et al., 1996; *Demant* et al., 1998) were identified in the investigated basement rocks from Site 1201. The natrolite group zeolites display large chemical variability in terms of Ca and Na contents, from almost pure natrolite, through mesolite and thomsonite, to almost pure scolecite (Table 2; Fig. 6A). The most variable compositions are identified in zeolites filling amygdules and replacing plagioclase, while zeolites within the groundmass display limited variations, from the thomsonite toward scolecite end-members. Very large chemical variability was detected in zeolites filling a single amygdule: an example is the zeolite filling shown in the photomicrograph of Fig. 3B, with Na

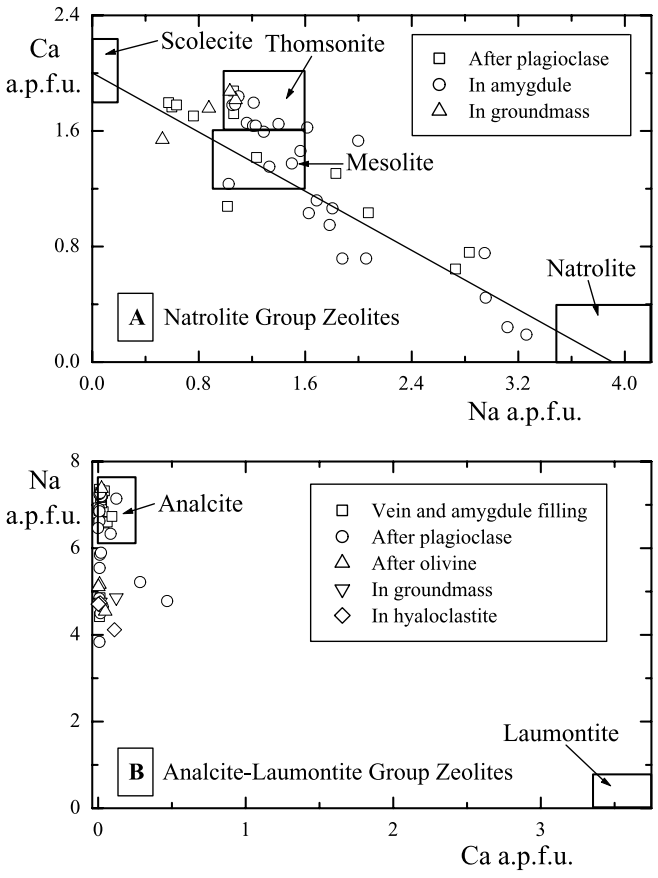

Fig. 6. Discrimination diagrams for zeolites (data from Table 2). **A** Natrolite group zeolites. Fields for end-members natrolite, thomsonite, mesolite and scolecite from *Alt* et al. (1986). **B** Analcite–laumontite group zeolites. Fields for end-members analcite and laumontite from *Deer* et al. (1992)

ranging from 3.3 (natrolite) to 1.7 (mesolite) a.p.f.u.. Similar wide compositional ranges were reported in a single vein by *Alt* et al. (1986).

The analcite composition is generally that of the pure $Na[AlSiO_6] \cdot H_2O$ component, but in some cases a small amount of Ca (i.e., laumontite component) was detected (Table 2). The analysis of analcite replacing plagioclase along with secondary alkali-feldspar displays less Na_2O and unusually high K_2O contents with respect to the other analcite analyses, as visible in the diagram of Fig. 6B. Tiny acicular crystals of manganese oxide were found inter-grown with analcite in a vein crosscutting basalt of the uppermost core (195-1201D-45R5, 103–107 cm). The manganese oxide probably originated from the sedimentary cover by leaching processes.

Alkali-feldspar

Plagioclase in the basalts from Site 1201 is often fully or partially replaced by secondary alkali-feldspar (Table 3), frequently intergrown with analcite. Secondary alkali-feldspar displays a wide range of compositions, from pure sanidine ($Or_{99}Ab_1$), through Na-rich sanidine ($Or_{47}Ab_{53}$), to anorthoclase, approaching the composition of albite ($Or_{16}Ab_{83}An_1$). In a few cases, plagioclase is slightly altered to Fe–K-richer compositions, thereby being displaced from the primary trend (Table 3).

Carbonates

Secondary carbonates occur in several investigated basalt samples. Their composition is dominated by the $CaCO_3$ component (always higher than 95%), with minor $MgCO_3$ and traces of $[Fe + Mn]CO_3$ components (Table 3). This is different from what has been observed in other altered MOR basalts, which include both pure $CaCO_3$ and Mg–Fe–Mn-carbonate varieties (*Tartarotti* et al., 1996; *Teagle* et al., 1996; *Hunter* et al., 1999; *Marescotti* et al., 2000; *Yatabe* et al., 2000). No significant compositional differences were detected in carbonate veins versus pseudomorphic substitution of primary phases, or within the groundmass. Raman spectroscopy determinations have allowed us to establish that all the carbonate which occurs in Site 1201 basement rocks, both as vein filling and replacement of former plagioclase and olivine phenocrysts, is calcite.

Glass

Altered volcanic glass is present in all the investigated rocks except the lowermost samples, although its abundance is a function of the degree of crystallinity of the sample. Palagonitization is diffuse throughout the entire basement sequence; nevertheless complete transformation to palagonite (i.e., to smectites; see *Zhou* and *Fyfe*, 1989) was never achieved. Indeed, several EMP analyses conducted on altered glass in samples from Site 1201 have revealed very variable compositions, particularly in terms of Fe, Ca and alkalis contents (some representative analyses are given in Table 3). These are thought to be mixtures of poorly crystallized clay minerals, carbonates and zeolites, especially analcite, but the analyses always have

Table 3. *Representative microprobe analyses of secondary alkali-feldspars, altered glass and carbonates. Formulae of alkali-feldspar and plagioclase calculated on the basis of 32 oxygens, assuming all Fe as* Fe^{3+}. b.d.l. *below detection limit.* * *as determined by Raman spectroscopy*

Label	110-5-5	117-16-3	115-127-2	114-14-6	131-51-4	117-17-3	110-9-2	Label	114-14-4	108-120-1	131-55-4	141-125-5
Occurrence	after Pl	after Pl	after Pl	after Pl	after Pl	hyaloclastite	spherulitic matrix	Occurrence	after Pl	in matrix	after Ol	in vein
Type	Sanidine	Sanidine	Sanidine	Anorthoclase	Altered plagioclase	Altered glass shard	Altered glass	Type	Calcite*	Calcite*	Calcite*	Calcite*
SiO_2	64.85	65.18	63.96	61.53	53.80	46.23	47.69					
TiO_2	0.02	b.d.l.	0.04	b.d.l.	0.07	0.50	0.31					
Al_2O_3	17.82	18.38	19.12	22.35	27.47	15.20	17.10					
FeO	0.13	0.05	0.09	b.d.l.	0.86	13.87	5.85	FeO	0.04	0.09	0.32	b.d.l.
MnO	b.d.l.	b.d.l.	b.d.l.	b.d.l.	b.d.l.	0.15	0.13	MnO	0.01	0.04	b.d.l.	b.d.l.
MgO	b.d.l.	b.d.l.	b.d.l.	b.d.l.	0.59	4.90	3.80	MgO	b.d.l.	0.78	1.32	0.99
CaO	0.02	0.04	0.43	0.03	12.89	1.89	8.11	CaO	55.98	55.44	54.78	55.74
Na_2O	0.13	0.26	0.36	6.98	3.25	0.15	1.55	Na_2O	b.d.l.	b.d.l.	b.d.l.	0.02
K_2O	16.28	16.59	15.69	9.42	1.37	5.36	0.50	K_2O	0.04	0.01	0.02	b.d.l.
Sum	99.26	100.52	99.68	100.31	100.39	88.25	85.04	Sum	56.07	56.36	56.45	56.75
Si	12.069	11.999	11.851	11.226	9.779							
Ti	0.003	0.000	0.006	0.000	0.010							
Al	3.910	3.989	4.176	4.807	5.885			$FeCO_3$	0.06	0.14	0.52	0.00
Fe^{3+}	0.020	0.008	0.013	0.000	0.131			$MnCO_3$	0.02	0.07	0.00	0.00
Mg	0.000	0.000	0.000	0.000	0.160			$MgCO_3$	0.00	1.62	2.76	2.07
Ca	0.003	0.009	0.085	0.005	2.510			$CaCO_3$	99.91	98.95	97.78	99.49
Na	0.048	0.091	0.128	2.468	1.144			Na_2CO_3	0.00	0.00	0.00	0.04
K	3.865	3.896	3.708	2.192	0.317			K_2CO_3	0.06	0.02	0.03	0.00
Total cations	19.918	19.992	19.967	20.697	19.935			Sum	100.05	100.81	101.10	101.60
An mol%	0.09	0.21	2.16	0.11	63.19							
Ab mol%	1.22	2.28	3.27	52.91	28.81							
Or mol%	98.69	97.50	94.57	46.99	7.99							

a poor stoichiometry. This latter feature is typical for many examples of altered basaltic glass (*Honnorez*, 1981; *Zhou* and *Fyfe*, 1989; *Pichler* et al., 1999).

Discussion and conclusions

The secondary mineral association present in the basement rocks from Site 1201, is dominated by Fe–Mg–K-clay minerals, natrolite group zeolites and analcite, and calcite. This mineral paragenesis is typical of very-low grade metamorphism of basic rocks (*Frey* and *Robinson*, 1999). The absence of other secondary minerals such as chlorite, epidote and albite constrains the temperature of the alteration to below 100–150 °C, at pressure not higher than 3 kbar (*Alt* and *Honnorez*, 1984; *Alt* et al., 1986; *Liou* et al., 1985; *Shikazono* et al., 1995; *Laverne* et al., 1996; *Teagle* et al., 1996; *Demant* et al., 1998; *Alt*, 1999; *Pichler* et al., 1999; *Marescotti* et al., 2000; *Porter* et al., 2000; *Chipera* and *Apps*, 2001). From the textural relationships among the secondary minerals found in the investigated samples, and from their chemical features, it is possible to infer the evolution history and conditions of the basement alteration.

Evolution history of basement alteration

The volcanic glass is likely the first phase to be altered, due to the lack of a well-developed crystal structure, making it highly susceptible to early alteration. Cooling induced fractures and vesicles of the basalts were lined and filled with abundant clay minerals, precipitated by circulating seawater, saturated in aluminum provided by the breakdown of plagioclase phenocrysts and microphenocrysts. The latter were partially or almost completely replaced by alkali-feldspar (from K- to Na-rich), natrolite group zeolites and analcite, in addition to glauconite, in various combinations. Olivine phenocrysts and microphenocrysts were always completely replaced by ''iddingsite'' or ''iddingsite''–glauconite–saponite mixtures, and rarely also by analcite and/or calcite, the latter two occurring later than clay minerals.

The simultaneous occurrence of secondary K–Na-feldspar and either analcite or natrolite group zeolites as patches within former plagioclase laths suggests that the alteration proceeded by a mechanism of dissolution–precipitation from hydrothermal seawater-derived fluid, rather than by ion-exchange. Seawater must have been the main supplier of potassium and/or sodium for the precipitation of alkali-feldspar and the abundant natrolite group zeolites and analcite.

Veins commonly have clay mineral linings and Na-zeolite fillings, thus indicating that the latter phase crystallized later. Similarly, amygdules may have Na–Ca-zeolite fillings and only very thin clay mineral linings; in other cases, much of the amygdule is filled with clay minerals, with or without a small zeolite core. The latter type of amygdules, although present in all cores, is mostly distributed in alteration halos around larger veins filled with either sedimentary inter-pillow material including hyaloclastite fragments, and/or calcite (in the uppermost cores, e.g., 195-1201D-46R-1 and 46R-5). In these amygdules, clay minerals are zoned in color from yellow-green to red to brown from rim to core, and the composition varies accordingly from glauconite to either ''iddingsite'' or clay mineral mixtures. Extreme zoning from glauconite with $Fe/(Fe + Mg)$ ratio of 0.7 to virtually pure

$Fe(O, OH)_x$ with $Fe/(Fe + Mg)$ ratio of 0.9 is not uncommon. Only in few cases, the reverse was found: one of the rare Al-saponite ($Fe/[Fe + Mg] = 0.23$) detected by EMPA was found at the core of a clay patch with a glauconite rim ($Fe/[Fe + Mg] = 0.60$). The latter observations have some implications for the alteration conditions that will be discussed later.

A 2 mm-wide vein with coarse euhedral crystals of calcite cemented by anhedral analcite, disseminated by MnO, was found in one of the uppermost cores (195-1201D-45R-5), suggesting that analcite crystallized later than calcite. However, in one deeper core (195-1201D-54R-1), two crosscutting veins were filled with analcite first and calcite later, and most calcite veins have thin linings of clay minerals and/or Fe staining, suggesting that carbonate is indeed the later phase. Moreover, in several cases, veins of analcite/calcite cut plagioclase phenocrysts already altered to K-feldspar (Fig. 3C, D), pseudomorphs of olivine (Fig. 3E) and clay minerals veins (Fig. 3F).

From all the above mutual relationships, it can be concluded that secondary minerals likely crystallized in the following sequence: clay minerals, ''iddingsite'', and their mixtures – Na-zeolites–calcite. The latter two minerals are undoubtedly the late-crystallizing phases in Site 1201 basement rocks, as observed in altered oceanic basalt sequences elsewhere (*Alt* et al., 1996; *Hunter* et al., 1999; *Marescotti* et al., 2000).

Physico-chemical conditions of hydrothermal alteration

It has been demonstrated that the composition of secondary clay minerals, and their association with other secondary minerals such as zeolites, sulfides and carbonates, can reveal whether the alteration occurred under oxidizing or reducing conditions, which is a direct consequence of the fluid/rock mass ratio. For instance, *Alt* and *Honnorez* (1984), *Alt* et al. (1986, 1996), *Laverne* et al. (1996), *Marescotti* et al. (2000) and *Schramm* et al. (2002) have shown cases in which the alteration of basaltic sequences have proceeded from oxidizing conditions first, to reducing conditions later. Under initial oxidizing conditions abundant celadonite, $Fe(O, OH)_x$, and celadonite-$Fe(O, OH)_x$ mixtures precipitate, whereas saponite, sulfides and calcite characterize later alteration under reducing conditions. The transition from oxidizing conditions to reducing conditions would be a direct consequence of the progressive isolation of the basement from the open circulation of seawater with increasing distance from the ridge axis and ageing of the oceanic crust, causing a decrease in the fluid/rock mass ratio (*Alt*, 1999). Following the procedure carried out by *Marescotti* et al. (2000), the composition of clay minerals, glauconite, Al-saponite, Fe-beidellite and their mixtures, as well as Fe-oxyhydroxides occurring in Site 1201 basalts are plotted in the ternary diagram Fe–Mg–K (Fig. 7). The diagram confirms that the main alteration of Site 1201 basement rocks occurred under oxidizing conditions, given the abundance of Fe- and K-rich clay minerals (glauconite) and Fe-oxyhydroxides in the rocks throughout the sequence. This inference implies a high seawater/rock ratio that exists only in an open-system hydrothermal circulation; the high L.O.I. of most of the investigated rocks (0.9–6.6 wt.%; *Salisbury* et al., 2002) is a confirmation of this implication. K-bearing clay minerals, such as celadonite and nontronite, and mixtures of

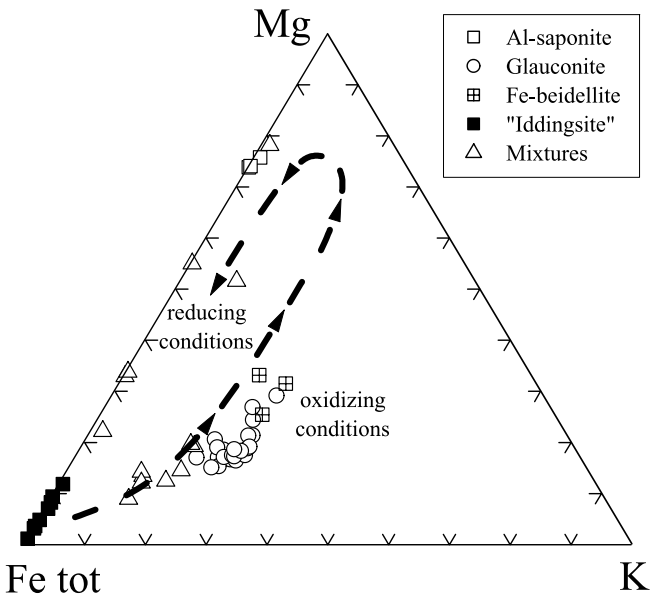

Fig. 7. Ternary plot Fe_{tot}–Mg–K for clay minerals, ''iddingsite'' and mixtures. The dashed curve illustrates the alteration path from oxidizing to progressively reducing conditions (after *Marescotti* et al., 2000)

$Fe(O, OH)_x$ and clay minerals form under highly oxidizing conditions at temperatures in the range 30–60 °C (*Seyfried* and *Bischoff*, 1979; *Alt*, 1988; *Clauer* and *Chaudhuri*, 1995; *Chipera* and *Apps*, 2001). Such a range of temperatures can be inferred for the formation of the abundant glauconite and ''iddingsite'' of Site 1201 altered basalts.

The open-system condition can persist for tens of millions of years if a volcanic pile remains exposed to the oxygenated seawater, e.g. when sedimentation rate is low (*Baker* et al., 1991). This must have been the case at Site 1201, where red claystones were deposited in a quiescent marine environment on top of the basaltic layer (*Salisbury* et al., 2002). However, in contrast to other case-studies (*Zierenberg* et al., 1995; *Alt* et al., 1996; *Marescotti* et al., 2000; *Schramm* et al., 2002), only minor Al-saponite is present in basalts from Site 1201. Al-saponite is identified as a late-stage mineral only in one case, and lacks accompanying sulfides, which typically occur in MORB altered under reducing conditions. Apparently, only the sparse, late-crystallized calcite would confirm that an alteration phase occurred under reducing conditions. Indeed, even though the two polymorphs of $CaCO_3$ do not necessarily imply particular redox conditions, aragonite is more typical of oxidizing environments, whereas calcite is much more commonly observed in mineral associations including saponite and sulfides, formed at low f_{O_2} (*Alt* and *Honnorez*, 1984; *Alt*, 1993; *Alt* et al., 1986, 1996; *Tartarotti* et al., 1996; *Teagle* et al., 1996; *Marescotti* et al., 2000). Moreover, natrolite group zeolites and analcite, which are inferred to be late crystallizing phases in the Site 1201 basement, are also thought to precipitate under reducing conditions (*Alt* and *Honnorez*, 1984).

In summary, alteration of the West Philippine Basin basement at Site 1201 has mainly occurred under open-system, oxidizing conditions, with a high seawater/basalt ratio, at temperatures in the range 30–60 °C, and probably for a time long enough to allow all the fractures and vesicles to become sealed by deposition of

secondary Fe- and K-smectites. Then, pelagic sedimentation progressively buried the volcanic pile with red clays, providing the manganese precipitated as oxide in the veins of the uppermost basalt of the volcanic pile. Moreover, the altered, very Ca-rich, but Mg–K-sulfate-poor water circulating within the lowermost turbidite and red clay sedimentary layers (*Salisbury* et al., 2002) may have supplied the calcium and sodium for precipitation of late-stage natrolite group zeolites, analcite and calcite to the isolated basement, although not favoring precipitation of sulfides. $\delta^{18}O$ data on altered basalts from other oceanic sites constrain the temperature of precipitation of Ca-carbonates to within about 70 °C (*Teagle* et al., 1996; *Hunter* et al., 1999; *Yatabe* et al., 2000). Also, natrolite group zeolites and analcite start to precipitate at T above ca. 70 °C (*Chipera* and *Apps*, 2001). Thus, it can be hypothesized that a late alteration phase must have occurred at Site 1201 at temperatures of about 70 °C, consistently with the temperature of 65.2 °C inferred for interstitial water at the base of the sedimentary sequence (*Salisbury* et al., 2002). Further investigation, including geochemical and isotopic studies on bulk rocks and mineral separates, would be necessary to refine the assessment of the physico-chemical conditions of alteration of Site 1201 basement proposed here, and to estimate the chemical changes involved in the process.

Acknowledgements

We are grateful to the Master and crew of R/V JOIDES Resolution, as well as to all the Leg 195 Scientific Party, who made Leg 195 a scientific success and unforgettable experience. *P. Spadea* (University of Udine) is warmly thanked for having encouraged and provided opportunity to *M.D.*, through the Italian ODP section of C.N.R., to participate in Leg 195. The assistance and cooperation of *R. Carampin* during collection of microprobe electron data at Padova is gratefully acknowledged. *M. L. Frezzotti* (Dipartimento di Scienze della Terra, University of Siena, Italy) and the P.N.R.A. (Progetto Nazionale di Ricerche in Antartide, C.N.R., Italy) are sincerely thanked for the Raman spectroscopy determinations on carbonates. We warmly acknowledge *J. Alt* and *P. Tartarotti* for their helpful comments and suggestions which greatly improved the manuscript, as well as *J.-P. Eissen* for his skillful editorial activity. This research has been funded by "Ricerca Dipartimentale 2002" grants (to *M. D.*). We wish to thank *O. R. Clausen* (University of Aarhus) and the Danish Science Foundation for financial support, and we would like to extend special thanks to *N. Mikkelsen* (GEUS), for her optimism and generous funds to *M. B. K.*, making this joint post-cruise project possible.

References

Agrinier P, Laverne C, Tartarotti P (1995) Stable isotope ratios (oxygen, hydrogen) and petrology of hydrothermally altered dolerites at the bottom of the sheeted dike complex of Hole 504B. In: *Erzinger J, Becker K, Dick HJB, Stokking* LB (eds) Proc ODP Sci Res 137/140: 99–106

Alt JC (1988) Hydrothermal oxide and nontronite deposits on seamounts in the eastern Pacific. Marine Geol 81: 227–239

Alt JC (1999) Very low-grade metamorphism of basic igneous rocks. In: *Frey M, Robinson D* (eds) Low-grade metamorphism. Blackwell Science, London, pp 169–201

Alt JC, Honnorez J (1984) Alteration of the upper oceanic crust, DSDP site 417: mineralogy and chemistry. Contrib Mineral Petrol 87: 149–169

Alt JC, Honnorez J, Laverne C, Emmermann R (1986) Hydrothermal alteration of a 1 km section through the upper oceanic crust, Deep Sea Drilling Project Hole 504B: mineralogy, chemistry, and evolution of seawater-basalt interactions. J Geophys Res 91: 10309–10335

Alt JC, Kinoshita H, Stokking LB et al. (1993) Proc ODP Initial Report, College Station, TX 148

Alt JC, Teagle DAH (2003) Hydrothermal alteration of upper oceanic crust formed at a fast-spreading ridge: mineral, chemical, and isotopic evidence from ODP Site 801. Chem Geol 201: 191–211

Alt JC, Teagle DAH, Laverne C, Vanko DA, Bach W, Honnorez J, Becker K, Ayadi M, Pezard PA (1996) Ridge flank alteration of upper ocean crust in the eastern Pacific: synthesis of results for volcanic rocks of Holes 504B and 896A. In: *Alt JC, Kinoshita H, Stokking LB, Michael PJ* (eds) Proc ODP Sci Res 148: 435–450

Alt JC, Zuleger E, Erzinger J (1995) Mineralogy and stable isotopic compositions of the hydrothermally altered lower sheeted dike complex, Hole 504B, Leg 140. In: *Erzinger J, Becker K, Dick HJB, Stokking LB* (eds) Proc ODP Sci Res 137/140:155–166

Andrews AJ (1980) Saponite and celadonite in Layer 2 basalts, DSDP Leg 37. Contrib Mineral Petrol 73: 323–340

Bach W, Alt JC, Niu Y, Humphris SE, Erzinger J, Dick HJB (2001) The geochemical consequences of late-stage low-grade alteration of lower ocean crust at the SW Indian Ridge: results from ODP Hole 735B (Leg 176). Geochim Cosmochim Acta 65: 3267–3287

Baker PA, Stout PM, Kastner M, Elderfield H (1991) Large-scale lateral advection of seawater through oceanic crust in the central equatorial Pacific. Earth Planet Sci Lett 105: 522–533

Buckley HA, Bevan JC, Brown KM, Johnson LR, Farmer VC (1978) Glauconite and celadonite: two separate mineral species. Mineral Mag 42: 373–382

Chipera SJ, Apps JA (2001) Geochemical stability of natural zeolites. In: *Bish DL, Ming DW* (eds) Natural zeolites: occurrence, properties, applications. Mineralogical Society of America and the Geochemical Society, Washington, DC, pp 117–161 (Rev Mineral Geochem 45)

Clauer N, Chaudhuri S (1995) Clays in crustal environment: isotope dating and tracing. Springer, Berlin Heidelberg New York Tokyo, pp 359

D'Antonio M, Kristensen MB (2004) Data report: electron microprobe investigation on primary minerals of basalts from Site 1201. In: *Salisbury MH, Shinohara M, Richter C* (eds) Proc ODP Sci Res (in press)

Deer WA, Howie RA, Zussman J (1992) An introduction to the rock-forming minerals, 2nd edn. Longman Scientific and Technical, Harlow, 696 pp

Demant A, Münch P, Romeuf N, Morata D (1998) Distribution and chemistry of secondary minerals (zeolites and clay minerals) from Hole 917A, Southeast Greenland margin. In: *Saunders AD, Larsen HC, Wise SW Jr* et al. (eds) Proc ODP Sci Res 152: 417–424

Deschamps A, Lallemand S, Dominguez S (1999) The last spreading episode of the West Philippine Basin revisited. Geophys Res Lett 26: 2073–2076

Deschamps A, Okino K, Fujioka K (2002) Late amagmatic extension along the central and eastern segments of the West Philippine Basin fossil spreading axis. Earth Planet Sci Lett 203: 277–293

Fehn U, Green KE, Von Herzen RP, Cathles LM (1983) Numerical models for the hydrothermal field at the Galapagos spreading center. J Geophys Res 88: 1033–1048

Frey M, Robinson D (eds) (1999) Low-grade metamorphism. Blackwell Science, London, 313 pp

Fujioka K, Okino K, Kanamatsu T, Ohara Y, Ishizuka O, Haraguchi S, Ishii T (1999) Enigmatic extinct spreading center in the West Philippine backarc basin unveiled. Geology 27: 1135–1138

Hall R (2002) Cenozoic geological and plate tectonic evolution of SE Asia and the SW Pacific: computer-based reconstructions, model and animations. J Asian Earth Sci 20: 353–431

Hall R, Ali JR, Anderson CD, Baker SJ (1995) Origin and motion history of the Philippine Sea Plate. Tectonophysics 251: 229–250

Hilde TWC, Lee C-S (1984) Origin and evolution of the West Philippine Basin: a new interpretation. Tectonophysics 102: 85–104

Honnorez J (1981) The ageing of the oceanic crust at low temperature. In: *Emiliani C* (ed) The Sea, vol 7. The oceanic lithosphere. Wiley, New York, pp 525–587

Humphris SE, Thompson G (1978a) Hydrothermal alteration of oceanic basalts by seawater. Geochim Cosmochim Acta 42: 107–125

Humphris SE, Thompson G (1978b) Trace element mobility during hydrothermal alteration of oceanic basalts. Geochim Cosmochim Acta 42: 127–136

Hunter AG, Kempton PD, Greenwood P (1999) Low-temperature fluid-rock interaction – an isotopic and mineralogical perspective of upper crustal evolution, eastern flank of the Juan de Fuca Ridge (JdFR), Leg 168. Chem Geol 155: 3–28

Hussong D, Uyeda S (1981) Tectonic processes and the history of the Mariana arc: a synthesis of the results of Deep Sea Drilling Project Leg 60. In: *Lee M, Powell R* (eds) Init Rept DSDP 60: 909–929

Laverne C, Agrinier P, Hermitte D, Bohn M (2001) Chemical fluxes during hydrothermal alteration of a 1200-m long section of dikes in the oceanic crust, DSDP/ODP Hole 504B. Chem Geol 181: 73–98

Laverne C, Belarouchi A, Honnorez J (1996) Alteration mineralogy and chemistry of the upper oceanic crust from Hole 896A, Costa Rica rift. In: *Alt JC, Kinoshita H, Stokking LB, Michael PJ* (eds) Proc ODP Sci Res 148: 151–170

Laverne C, Vanko DA, Tartarotti P, Alt JC (1995) Chemistry and geothermometry of secondary minerals from the deep sheeted dike complex, Hole 504B. In: *Erzinger J, Becker K, Dick HJB, Stokking LB* (eds) Proc ODP Sci Res 137/140: 167–189

Li G, Peacor DR, Coombs DS, Kawachi Y (1997) Solid solution in the celadonite family: the new minerals ferroceladonite, $K_2Fe^{2+}{}_2Fe^{3+}{}_2Si_8O_{20}(OH)_4$, and ferroaluminoceladonite, $K_2Fe^{2+}{}_2Al_2Si_8O_{20}(OH)_4$. Am Mineral 82: 503–511

Liou JG, Maruyama S, Cho M (1985) Phase equilibria and mineral parageneses of metabasites in low-grade metamorphism. Mineral Mag 49: 321–333

Lister CRB (1982) 'Active' and 'passive' hydrothermal systems in the ocean crust. In: *Fanning KA, Manheim FT* (eds) The dynamic environment of the Ocean floor. DC Heath, Lexington, MA, pp 441–470

Marescotti P, Vanko DA, Cabella R (2000) From oxidizing to reducing alteration: mineralogical variations in pillow basalts from the East Flank, Juan de Fuca Ridge. In: *Fisher A, Davies EE, Escutia C* (eds) Proc ODP Sci Res 168: 119–136

McPhie J, Doyle M, Allen R (1993) Volcanic textures: a guide to interpretation of texture in volcanic rocks. CODES, University of Tasmania, 198 pp

Mottl MJ, Wheat G (1994) Hydrothermal circulation through mid-ocean ridge flanks: fluxes of heat and magnesium. Geochim Cosmochim Acta 58: 2225–2237

Okino K, Ohara Y, Kasuga S, Kato Y (1999) The Philippine Sea: new survey results reveal the structure and the history of the marginal basins. Geophys Res Lett 26: 2287–2289

Passaglia E (1970) The crystal chemistry of chabazites. Am Mineral 55: 1278–1301

Peacor DR (1992) Diagenesis and low-grade metamorphism of shales and slates. Mineral Soc Am Rev Mineral 27: 335–380

Pichler T, Ridley WI, Nelson E (1999) Low-temperature alteration of dredged volcanics from the Southern Chile Ridge: additional information about early stages of seafloor weathering. Marine Geol 159: 155–177

Porter S, Vanko DA, Ghazi M (2000) Major and trace element compositions of secondary clays in basalts altered at low temperature, eastern flank of the Juan de Fuca Ridge. In: *Fisher A, Davies EE, Escutia C* (eds) Proc ODP Sci Res 168: 149–158.

Rangin C, Silver EA, Tamaki K (1995) Closure of western Pacific marginal basins: rupture of the oceanic crust and the emplacement of ophiolites. In: *Taylor B, Natland J* (eds) Active margins and marginal basins of the Western Pacific. American Geophysical Union, Washington, DC, 405–417 (Geophys Monogr 88)

Salisbury MH, Shinohara M, Richter C et al. (2002) Seafloor observatories and the Kuroshio current – Sites 1200–1202. Proc ODP Init Rept 195: pp 1–233 [CD-ROM] Available from: Ocean Drilling Program, Texas A&M University, College Station TX 77845-9547, USA

Schramm B, Devey CW, Gillis KM, Lackschewitz K (2002) Low temperature alteration of basalts during the last 9 Ma at 14°15′S on the South East Pacific Rise. EOS Trans AGU 83(47), Fall Meet Suppl, Abstr V61B-1360

Seyfried WE Jr, Bischoff JL (1979) Low temperature basalt alteration by seawater: an experimental study at 70 °C and 150 °C. Geochim Cosmochim Acta 43: 1937–1947

Shikazono N, Utada M, Shimizu M (1995) Mineralogical and geochemical characteristics of hydrothermal alteration of basalt in the Kuroko mine area, Japan: implications for the evolution of a Back Arc Basin hydrothermal system. Appl Geochem 10: 621–642

Tartarotti P, Vanko DA, Harper GD, Dilek Y (1996) Crack-seal veins in upper layer 2 in Hole 896A. In: *Alt JC, Kinoshita H, Stokking LB, Michael PJ* (eds) Proc ODP Sci Res 148: 281–288

Teagle DAH, Alt JC, Bach W, Halliday AN, Erzinger J (1996) Alteration of upper crust in a ridge-flank hydrothermal upflow zone: mineral, chemical, and isotopic constraints from Hole 896A. In: *Alt JC, Kinoshita H, Stokking LB, Michael PJ* (eds) Proc ODP Sci Res 148: 119–150

Teagle DAH, Alt JC, Chiba H, Humphris SE, Halliday AN (1998) Strontium and oxygen isotopic constraints on fluid mixing, alteration and mineralization in the TAG hydrothermal deposit. Chem Geol 149: 1–24

Wetzel LR, Raffensperger JP, Shock EL (2001) Prediction of hydrothermal alteration within near-ridge oceanic crust from coordinated geochemical and fluid flow models. J Volcanol Geotherm Res 110: 319–342

Yatabe A, Vanko DA, Ghazi AM (2000) Petrography and chemical compositions of secondary calcite and aragonite in Juan de Fuca Ridge basalts altered at low temperature. In: *Fisher A, Davies EE, Escutia C* (eds) Proc ODP Sci Res 168: 137–149

Zierenberg RA, Schiffman P, Jonasson I, Tosdal R, Pickthorn W, McClain J (1995) Alteration of basalt hyaloclastite at the off-axis Sea Cliff hydrothermal field, Gorda Ridge. Chem Geol 126: 77–99

Zhou Z, Fyfe WS (1989) Palagonitization of basaltic glass from DSDP Site 335, Leg 37: textures, chemical composition, and mechanism of formation. Am Mineral 74: 1045–1053

Authors' addresses: *M. D'Antonio* (corresponding author), Dipartimento di Scienze della Terra, University Federico II, L.go S. Marcelllino 10, 80138 Napoli, Italy, e-mail: masdanto@unina.it; *M.B. Kristensen*, Department of Earth Sciences, University of Aarhus, C.F. Møllers Allé Bygn. 110, DK-8000 Århus, Denmark, e-mail: mette.bundgaard@geo.au.dk